HYDROTHERMAL SYNTHESIS AND CHARACTERIZATION OF Co$_{0.5}$Zn$_{0.5}$Fe$_2$O$_4$ NANO-MATERIAL AND EVALUATION OF ITS PHOTO-CATALYTIC ACTIVITY UNDER VISIBLE LIGHT IRRADIATION

A. RAZA[a], A. AZAM[b], M. S. SAEED[a], M. AHSAN[a], F. QAYYUM[a], M. YASEEN[a*]
[a] Department of Physics, University of Agriculture, Faisalabad 38040, Pakistan,
[b] Department of Physics, University of Education, Faisalabad Campus, Pakistan,

Cobalt zinc ferrite (Co$_{0.5}$Zn$_{0.5}$Fe$_2$O$_4$) nano-photocatalysts have been synthesized via hydrothermal technique with fine crystallinity. The above synthesized nano-photocatalysts (NPs) were characterized by XRD, SEM, EDX and UV−Vis photo-spectrometer. The efficiency of the above synthesized Co$_{0.5}$Zn$_{0.5}$Fe$_2$O$_4$ nanoparticles, as a catalyst for the photo degradation of toluidine blue O (TBO) dye, function of the ratio between the catalyst and the substrate, was studied after irradiation under visible light. The photo-catalytic activity of Co$_{0.5}$Zn$_{0.5}$Fe$_2$O$_4$ NPs under the visible-light irradiation was checked by the degradation rate of Toluidine Blue O (TBO). The results exhibited that an efficient interaction between the catalyst and the substrate took place to cause degradation of the dye. The degradation rate of TBO 94.3% was observed in 2 hours. The percentage of degradation of toluidine blue O (TBO) and total organic carbon (TOC) removal were reduced by only 8% and 14% under UV-vis light irradiation, respectively after five successive cycles.

1. Introduction

Synthetic dyes are major water contaminants and industrial pollutants in these days [1, 2]. Toxicity with intensive color to aquatic systems are the results of these textile waste water [3] Dyes are mostly resistant to physicochemical treatment methods for their destruction and degradation [4].

Traditional treatment process like coagulation and biochemical treatment process are insufficient to treat these kinds of wastewater because these organic dyes with their resultant waste solution are unpredictable in behavior. Nowadays, activated carbon adsorption process is an accepted practice for degradation of organic dyes but the high cost makes it unattractive. Effective de-colorization methods like Ozone and hypochlorite oxidations are not desirable because of expensive equipment as well as high operating cost and assurgent of secondary pollution from the residual chlorine [5].

Since the 1990s, advanced oxidation processes (AOPs) are the source of interest for the treatment of wastewater [6]. Theoretically, procreation of hydroxyl radicals (˙OH) in water is the base of advanced oxidation processes (AOPs). These hydroxyl radicals (˙OH) have the ability to oxidize unsaturated organic compounds like azo dyes. Ozonation, Fenton, photo-Fenton, wet oxidation, and photo-catalysis are some techniques of advanced oxidation processes (AOPs) [6-8].

Synthesis of semiconductor photo-catalysts have been gained considerable interest for the purpose of air purification and water disinfection [9–11]. A number of semiconductor oxides as photo-catalysts are synthesized these days. An extensive study has been carried out over cobalt-zinc ferrite because of its promising oxidizing power, chemical inertness and long-term stability against photo-chemical decay [12]. Though, practical use of these semiconductor oxides has become limited due to rapid re-combination of photo-generated electron-hole pairs. By decreasing the rate

---

*Corresponding author: myaseen_taha@yahoo.com

of electron-hole pair's recombination, the photonic efficiency of a photo-catalyst can be increased [12-14]. High magnetic permeability and low magnetic hysteresis loss make cobalt-zinc ferrite an important ferromagnetic material [12]. A simple and common ceramic process like co-precipitation is used to synthesis these ferrites. In this process, a high calcination of oxide and/or carbonates is involved. Their large and non-uniform size distribution, contamination, poor reproducibility and a need for the application of high temperature for production are their main disadvantages [15].

As reported in the literature, a number of methods are used to fabricate semiconductor oxide (called ferrites) including co-precipitation, sol–gel, mechano-chemical and hydrothermal method [16–21].

The hydrothermal method has several advantages over other conventional methods but low temperature of reaction is the main advantage. In fact, the hydrothermal method provides well crystallized and pure materials, consequently preventing additional thermal treatments. Moreover, the extremely high temperature is not a requirement for hydrothermal synthesis route. In other words, nano-structured materials can be synthesized via hydrothermal route in temperature range of 140-200 $^\circ$C, but the solid state technique requires a temperature of 800 $^\circ$C [22-26]. Sub-micro-metric and even nano-metric or nanostructured materials can possibly be obtained as offers by this characteristic [27].

The present study evaluates the photo-catalytic activity of Cobalt zinc ferrite ($Co_{0.5}Zn_{0.5}Fe_2O_4$) which was hydrothermally synthesized at 200 $^\circ$C within 4 hours. Their photo-catalytic activity was examined for degradation of Toluidine Blue O (TBO) dye. Size, shape structure and composition of the nanoparticles (NPs) were characterized by XRD, SEM and EDX. The photo-catalytic activity of $Co_{0.5}Zn_{0.5}Fe_2O_4$ NPs was investigated by degrading TBO dye under visible light irradiation.

2. Experimental Section

2.1 Synthesis of $Co_{0.5}Zn_{0.5}Fe_2O_4$ Nanoparticles

All the chemicals were purchased from S.C. Co. USA and were used without extra purification because of (99.9% purity). Chemicals used in the synthesis were $CoCl_2 \cdot 6H_2O$, $ZnCl_2$, $FeCl_3 \cdot 6H_2O$, and NaOH. For the synthesis of $Co_{0.5}Zn_{0.5}Fe_2O_4$ NPs by hydrothermal technique, a 0.5M solution of $CoCl_2 \cdot 6H_2O$ and $ZnCl_2$ were prepared by dissolving in 50mL sterile deionized water. Another solution was prepared by dissolving 1M of $FeCl_3 \cdot 6H_2O$ in 50mL sterile deionized water. These two solutions were homogenized by stirring at 65 $^\circ$C for 30 min using hot plate magnetic stirrer (55 rpm). A base solution of 3.5 M NaOH was used to increase the solution's pH nearby 10. During drop wise addition of base solution, homogeneous solution was continuously stirred until reddish brown precipitates were formed. Precipitates were placed into a Teflon-line autoclave and heated for 4 hours at 200 $^\circ$C. At room temperature, the autoclave was allowed to cool [28]. The filtration was done by using Grade 287 filter paper (GE Healthcare Life Sciences) and the residual precipitates were washed several time with deionized water until chlorides were completely removed from the disposed water and the pH of the residual precipitates reached 7. The filtered precipitates were dried for 2 h at 100 $^\circ$C. Consequently, the precipitate was grind in agate mortar and pestle and the calcined at 400 $^\circ$C. Fig. 1 shows the flow chart of experimental procedure of hydrothermal synthesis.
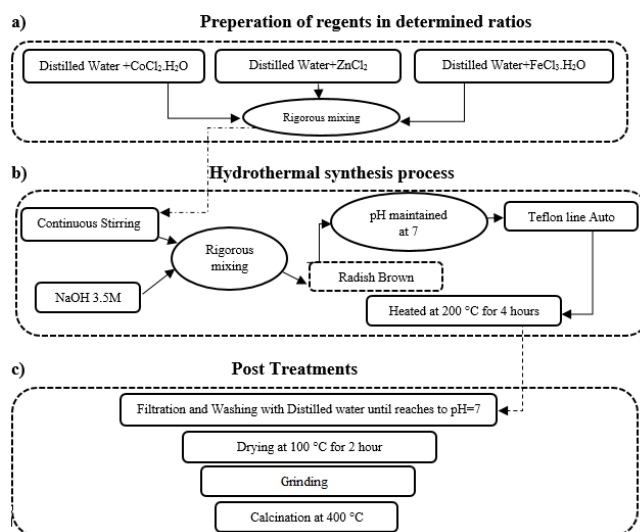
Fig. 1. Flow Chart of Experimental Procedure

Characterization

Analysis of the crystalline phase of $Co_{0.5}Zn_{0.5}Fe_2O_4$ nano-photocatalyst was done by X-ray diffractometer (Shimadzu XRD-6000, Japan) with Cu Kα radiation in the region $2\theta = 10°$ to $90°$ with a step size of $0.04°$. These patterns were compared with JCPDS file cards and peaks were characterized. The crystallite size was calculated by using Scherrer equation [29].

$$D = \frac{B\lambda}{\beta \, Cos\theta B} \qquad (2)$$

Where,

D is the crystallite size, B is the Scherer's constant (0.89), λ is the X-ray wavelength, β is the full-width at half-maximum (FWHM) of diffraction and θB is the Bragg's angle.

Scanning Electron Microscope (JEOL JSM 7401 F) was used to study the overall morphology of nano-photocatalyst. For morphological analysis, a gold coated specimen was used.

UV/Vis spectrophotometer (Macy UV-1900, china) was used to study the photo-catalytic degradation.

Photo-catalytic Reaction

The preparation of $Co_{0.5}Zn_{0.5}Fe_2O_4$ solution was done by mixing a certain amount of $Co_{0.5}Zn_{0.5}Fe_2O_4$ NPs into deionized water. The mixture was treated ultrasonically for 15-20 minutes. In the meantime, transparent and self-dispersed $Co_{0.5}Zn_{0.5}Fe_2O_4$ solution was formed.

For photo-degradation experiment, dye solution of the requisite volume was combined with the $Co_{0.5}Zn_{0.5}Fe_2O_4$ NPs solution. The combined solution was poured into a glass reactor and adsorption equilibrium was attained during continues stirring for 20 min in the absence of light [30]. Furthermore, The $Co_{0.5}Zn_{0.5}Fe_2O_4$ NPs/TBO solution was irradiated with UV-Visible light under constant stirring in presence of oxygen. A UV-Visible lamp (120 W) of visible light (190～900 nm) was used for photo-reaction process. In between photo-reaction, a small amount of $Co_{0.5}Zn_{0.5}Fe_2O_4$ NPs /TBO solution was isolated after every 20 min and centrifuged for 10 min and nano-photocatalyst was separated from $Co_{0.5}Zn_{0.5}Fe_2O_4$ NPs /TBO solution. The monitoring of TBO decomposition was done by evaluating the absorbance peak at $\lambda_{max} = 632 \pm 5$ nm. The commercially used Degussa P25 powder sample was tested as an assessment catalyst and the same procedure was followed for the blank reaction (without catalyst). TBO dye concentration (*C*) was

detected directly in the solution to measure the degradation before and after visible light irradiation.

The degradation % measured by equation [33]

$$D\% = \frac{A°-A}{A°} \times 100 \tag{1}$$

Where $A°$ is representing the absorbance of the mixture before degradation and A is the absorbance of the mixture after degradation. Reusability test of the same $Co_{0.5}Zn_{0.5}Fe_2O_4$ nano-photocatalyst was done repeatedly for 5 times.

Total organic carbon (TOC) abstraction was done and mineralization of TBO with $Co_{0.5}Zn_{0.5}Fe_2O_4$ nano-photocatalyst was estimated through TOC analyzer (Metash TOC-3000, China). Primarily, a decline in TOC was determined and then Concentration of TBO mineralization in the reaction solution was estimated.

2. Results

Characteristics of the $Co_{0.5}Zn_{0.5}Fe_2O_4$ nano-photocatalyst

The existence of the crystalline phase of $Co_{0.5}Zn_{0.5}Fe_2O_4$ nano-photocatalyst was confirmed by the XRD results. Well defined peaks are (1 1 1), (2 2 0), (2 2 2), (3 1 1), (4 0 0), (4 2 2), (5 1 1) and (4 4 0) of spinal structure can be observed in Figure 2. The strongest reflection of (3 1 1) plane represents cubic spinal structure. According to the *Fd3m* cubic spinel structure, the value of lattice constant "a" can be calculated from the utmost strong (3 1 1) reflection with the help of formula $(1/d_{hkl}^2 = (h^2+k^2+l^2)/a^2)$ [29]. The estimated particle size of $Co_{0.5}Zn_{0.5}Fe_2O_4$ nano-photocatalyst was about~16 nm as show in Table 1.

Table 1: Characterization data of XRD for $Co_{0.5}Zn_{0.5}Fe_2O_4$ nano-photocatalyst

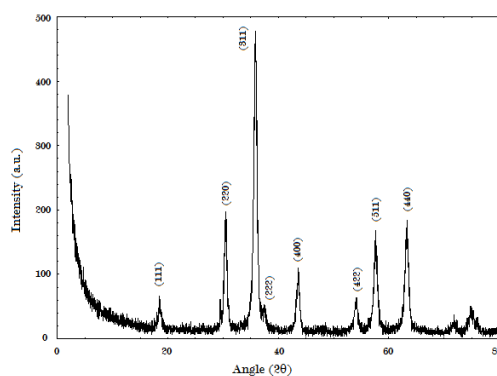| Ferrite composition	$Co_{0.5}Zn_{0.5}Fe_2O_4$
Lattice constant	8.38A°m
Volume	580.10(A°m)^3
Bulk density	~4.00 gm^{-3}
X-ray density	5.28 gm^{-3}
Crystallite size	~16 nm
Porosity	24.92 %

Fig. 2: XRD pattern of hydrothermally synthesized $Co_{0.5}Zn_{0.5}Fe_2O_4$ nano-photocatalyst.

According to SEM micrographs, the estimated average particle size of ten particles at ×10,000 magnification was ∼16 nm (Fig. 3). Moreover, SEM micrograph clearly shows the uniformity and particulate structural morphology of $Co_{0.5}Zn_{0.5}Fe_2O_4$ nano-photocatalyst. In quantitative analysis, energy dispersive X-ray spectroscopy (EDX) spectra (Figure 4) of the sample depicted the presence of Co, Zn, Fe and O in the samples. The EDX spectrum shows no traces of by-products. The starting materials for the synthesis of $Co_{0.5}Zn_{0.5}Fe_2O_4$ NPs were highly pure so no contamination is observed. Table 2 shows the chemical composition of $Co_{0.5}Zn_{0.5}Fe_2O_4$ nano-photocatalyst.

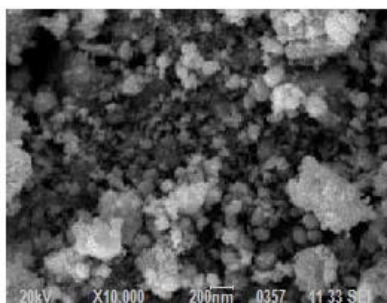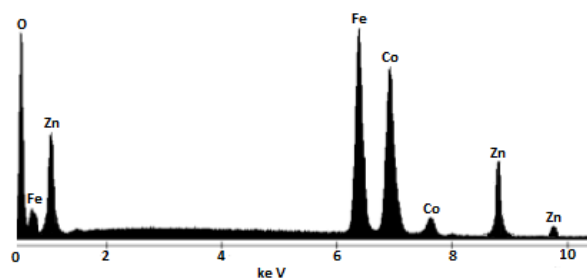*Fig. 3: SEM images for $Co_{0.5}Zn_{0.5}Fe_2O_4$ nano-photocatalyst*

Fig. 4: EDX pattern of synthesized $Co_{0.5}Zn_{0.5}Fe_2O_4$ nano-photocatalyst

Table 2. Elemental composition of the $Co_{0.5}Zn_{0.5}Fe_2O_4$ nano-photocatalyst.

Element Line	Weight %	Atomic %
O K	30.90	61.53
Fe K	49.87	27.80
Co K	10.6	5.62
Zn K	8.63	5.05
Total	100	100

Band gap Energy

The estimated band gap of $Co_{0.5}Zn_{0.5}Fe_2O_4$ NPs calculated from Tauc plot was 1.96 eV. For an efficient photocatalyst, the band gap must be narrow (up to 3.0 eV) to make use of the visible part of electromagnetic spectrum ($\lambda > 400$ nm). The calculated bandgap is in the narrow range of photo-catalyst, representing that the as-synthesized nano-photocatalyst can absorb visible light.

Absorbance Spectra of TBO Degradation

Absorption spectra in Fig. 6 shows that the intensity of a strong absorption band is gradually reducing at 632±5 nm for the TBO solution, which reveals that the distraction of bulky conjugated π system of the TBO dye molecules in the photo-assisted degradation. Fig.5 shows the

molecular formula, molecular weight, chemical structure and absorption maxima of TBO dye. For a period of 2 hrs. The absorbance spectra of TBO dye degradation is shown in Fig.6.
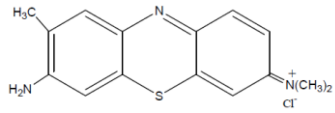
Name	Molecular Formula	Molecular Weight	Chemical Structure	λ_{max} (nm)
Toluidine Blue O	$C_{15}H_{16}N_3S \bullet Cl$	305.83		632

Fig. 5. Molecular Formula, Chemical Structure and absorption maxima of Toluidine Blue O
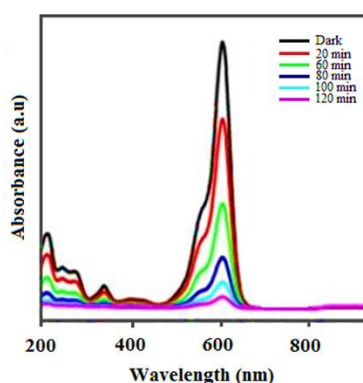

Fig. 6: Absorbance spectra of TBO degradation by $Co_{0.5}Zn_{0.5}Fe_2O_4$ nano-photocatalyst

Evaluation of Photo-catalytic Activity

It is well-known that the generation of electron-hole pairs is the base of photo-catalytic procedure. The band gap radiation can result in the redox reactions with adsorbed species over the catalysts surface. It is believed that the photo-catalytic degradation of a dye takes place in the following manners: When UV-Vis. radiation exposed over a catalyst, electrons become excited and due to this excitation promotion of these electrons in between valence to the conduction band take place. In result, a pair of electron-hole is created.

$$Co_{0.5}Zn_{0.5}Fe_2O_4 + hv \rightarrow Co_{0.5}Zn_{0.5}Fe_2O_4 \ (e_{cb}^- + h_{vb}^+) \qquad (3)$$

Where, e_{cb}^- represents the electrons in the conduction band (C.B) and h_{vb}^+ is showing the vacancy of electron in the valence band (V.B). Together these entities migrate on the surface of catalyst, where a redox reaction takes place with other species which presents on the catalyst surface. In many circumstances, h_{vb}^+ reacts with H_2O easily, which bounds on the catalyst surface and create hydroxyl radicals, however, e_{cb}^- reacts with O_2 and create O_2^- radicals. These electron and hole do not combine together.

$$H_2O + h_{vb}^+ \rightarrow {}^\bullet OH + H^+ \qquad (4)$$

$$O_2 + e_{cb}^- \rightarrow O_2^- \qquad (5)$$

These produced ${}^\bullet OH$ and O_2^- radicals react with the organic compound like dye to create additional species and consequently, responsible for the discoloration of this organic compound.

$$O_2^- + H^+ \rightarrow HO_2^\bullet \qquad (6)$$

$$H_2O_2 \rightarrow 2\,^{\bullet}OH \tag{7}$$

$$^{\bullet}OH + TBO \rightarrow Dye_{ox} \tag{8}$$

$$TBO + e_{cb}^{-} \rightarrow intermediates \rightarrow H_2O + CO_2 \tag{9}$$

It should be noted that if both water and dissolved oxygen molecules are present then all above mentioned steps in photo-catalysis are possible. Highly reactive hydroxyl radicals ($^{\bullet}OH$) might not be created in the absence of water molecules, which prevent the photo-degradation of organic molecules in liquid phase [32]. A possible mechanism of this photo-catalysis practice is illustrating by a schematic diagram in Figure 7.
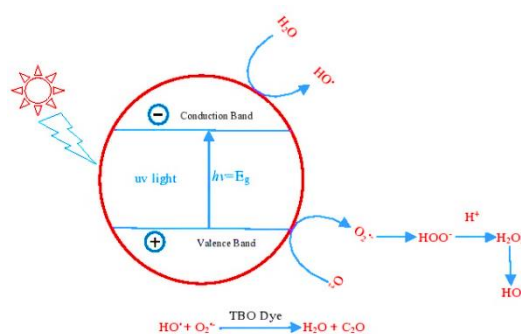

Fig. 7. Schematic diagram of possible mechanism of photocatalysis
process of TBO dye under visible light.

The Cobalt-substituted ferrite has metastable energy levels and narrow energy band gap which are generated within the energy gap that can transference the absorption to the visible region. Consequently, under visible light irradiation Co substituted ferrite can show better photo-catalytic performance.

The Decomposition rate of TBO dye was studied to assess the photo-catalytic activity with a cut-off filter ($\lambda \geq 420$ nm). A rapid decomposition of TBO was observed which shows the photo-catalytic activity of prepared photo-catalyst. Figure 8 is illustrating a comparison of degradation rates between TBO solution with catalyst, without catalyst and with Degussa P25. An approximate 94.3% degradation of dye solution was evaluated under visible light for $Co_{0.5}Zn_{0.5}Fe_2O_4$ NPs in 2 h Fig. 6.
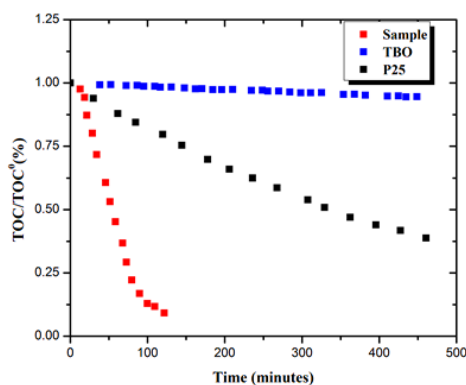

Fig. 8: Photo-catalytic degradation of the TBO under visible light irradiation
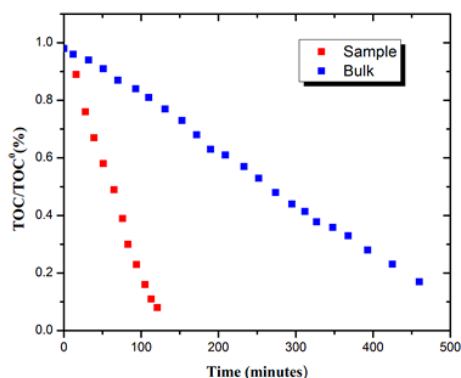*as a function of reaction time.*

Fig. 9: Photo-catalytic degradation of TBO under visible light
without catalyst and with Catalyst.

Previously [31] assessed the degradation rate of TBO by using $ZrFe_2O_5$ nanoparticles as catalyst under visible light irradiation. They have estimated 92% concentration of TBO mineralization after 140 minutes of visible light irradiation.

During dye degradation, Catalysis was take place over the surface region of $Co_{0.5}Zn_{0.5}Fe_2O_4$ NPs, so by enlarging its specific surface area, efficiency of the prepared photo-catalyst will be improved significantly. Decrease in particle size will cause significant increase in catalytic activity of a photo-catalysts but further decrease in particles size then critical size, will hamper the process [33]. The $Co_{0.5}Zn_{0.5}Fe_2O_4$ NPs act as a substrate and support e^- transfer reaction. In this reaction, reactants are absorbed over the surface of catalyst and therefore, the reactants gain an e^- and is reduced. As per electronic structure, the band potentials of $Co_{0.5}Zn_{0.5}Fe_2O_4$ NPs attain a straddling gap, which may make possible the transfer of charge carriers and reduce the electron-hole recombination. By reducing the electron-hole recombination, a superior photocatalytic performance can be ensured. Thus $Co_{0.5}Zn_{0.5}Fe_2O_4$ act as an efficient photo-catalyst through the electron transfer process in photo-catalytic reactions [31,34].

Stability Evaluation of $Co_{0.5}Zn_{0.5}Fe_2O_4$ Nano-photocatalyst.

For industrial applications, The Reusability and stability of catalyst are leading Priorities. Therefore, the reusability and stability of prepared nano-photocatalyst have been investigated. The nano-photocatalyst was used to photo-degrade the direct TBO dye repeatedly under UV-Vis light irradiation (Figure 9).
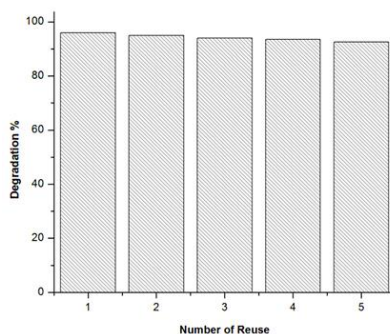

Fig. 10: Reusability and stability rate of $Co_{0.5}Zn_{0.5}Fe_2O_4$ nano-photocatalytic
in five consecutive tests

A steady photo-catalytic performance was shown by the synthesized $Co_{0.5}Zn_{0.5}Fe_2O_4$ nano-photocatalyst even after five successive cycles. The interesting point was that the prepared nano-photocatalyst remained active after five successive cycles. The prepared nano-photocatalyst

degraded 92.7% of the added TBO even on its fifth cycle (Figure 10). The percentage of toluidine blue O (TBO) and total organic carbon (TOC) removal were reduced by only 8% and 14% under UV-Vis light irradiation, respectively. Moreover, photo-catalytic performance indicates the high reusability and photo-stability against the visible light.

3. Conclusions

The $Co_{0.5}Zn_{0.5}Fe_2O_4$ nano-photocatalyst was synthesized by hydrothermal method. The synthesized material was characterized by XRD, SEM, EDX and UV/Vis photo spectrometer techniques. The particle size calculated by using sherrer formula was 16 nm and confirmed by SEM. The EDX revealed the presence of all the elements of the synthesized material. The photo-catalytic activity of the synthesized $Co_{0.5}Zn_{0.5}Fe_2O_4$ was studied by degradation rate of toluidine blue O (TBO) dye under UV-vis light irradiation. The Photo-catalytic measurements of synthesized NPs showed highly active and efficient output in very short irradiation time as compared to a standard commercially used Degussa P25. As-synthesised $Co_{0.5}Zn_{0.5}Fe_2O_4$ nano-photocatalyst also shows promising properties like reusability and photo-stability against the UV-Vis light irradiation.

Acknowledgement

References

[1] D. H., Brown, H.R., Hitz, and L., Schafer. Chemosphere, **10**, 245 (1981).

[2] A. A.,Vaidya, K.V., Datye. Colourage, **14**, 3 (1982).

[3] M. Muruganandham, M., Swaminathan. Dyes Pigments, **62**, 269 (2004).

[4] N. Daneshvar, M., Rabbani, N., Modirshahla and M.A., Behnajady. J. Hazard Mater. **118**, 155 (2005).

[5] P.K. Malik and S.K., Saha Sep. Purif Technol, **31**, 241 (2003).

[6] S. Caudo, G., Centi, C., Genovese and S., Perathoner. Appl. Catal. B: Environ. **70**, 437 (2007).

[7] E. Chamarro, E., Maeco and S., Esplugas. Water Res., **35**, 1047 (2001).

[8] E. Psillakis and D. Mantzavinos. J. Chem. Technol. Biotechnol., **79**, 431 (2004).

[9] X. Guangcan, W. Xinchen, L., Danzhen and F. Xianzhi. J. Photochem. Photobiol. 213-221 (2008).

[10] L., Qilin, M., Shaily, Y.L., Delina, B., Lena, V.L., Michael and L., Dong. Water Res. **42**, 4591 (2008).

[11] B. Detlef. Solar Energy, **77(5)**, 445 (2004).

[12] G. Fan, and J., Tong. Ind. Eng. Chem., **51**, 13639 (2012).

[13] S. Chen, L., Chen, S., Gao, and G., Cao. Mater. Chem. Phys. **98**, 116 (2006).

[14] C. W., Ku, W. Y., Shiang, T. C., Yao, and Y.L., Austin. J. Alloys Compd., **478**, 341 (2009).

[15] A. Angermann, E., Hartmann, and J., T¨Öpfer. Journal of Magnetism and Magnetic Materials, **322**, 3455 (2010).

[16] N. M., Deraz, and S., Shaban. J. Anal. Appl. Pyrol., **86**, 173 (2009).

[17] A. Alarifi, N.M., Deraz, and S., Shaban. J. Alloys Compd. **486**, 501 (2009).

[18] S. Ayyappan, J., Philip, and B., Raj. Mater. Chem. Phys., **115**, 712 (2009).

[19] A. Pradeep, P., Priyadharsini, and G., Chandrasekaran. J. Magn. Mater., **320**, 2774 (2008).

[20] B. Baruwati, R. K., Rana, and S. V., Manorama. J. Appl. Phys., vol. 101, p. 0143021 (2007).

[21] X. D., Li, W. S., Yang, F., Li, D. G., Evans, and X., Duan. J. Phys. Chem. Solids, **67**, 1286 (2006).

[22] S. Ifrah, A., Kaddouri and P., Gelin. CR Chimie, **10**, 1216-1226 (2007).

[23] D. Solís, T., López-Luke, and E., De la Rosa. J. Lumin., **129**, 449-455 (2009).

[24] D. R. Zhang, H. L., Liu, and R. H. Jin. J. Ind. Eng. Chem., **13**, 92-96 (2007).

[25] S. M. Wang, Q.S., Wang and Q. L., Wan. J. Cryst. Growth, **310**, 2439-2443(2008).

[26] R. Piticescu, C., Monty and D., Millers. Sensor Actuat B, **109**, 102-106 (2005).

[27] C. Kaya, J.Y., He, and X., Gu. Micropor Mesopor Mat., **54**, 37-49 (2002).

[28] E. Casbeer, Sharma, V. K., and Li, X. Z. Separation and Purification Technology, **87**, 1 (2012).

[29] B. D. Cullity. "Elements of X-ray Diffraction." Addison-Wesly Publishing Co. Inc., Chap. 14 (1976).

[30] M. Shahid, I., Shakir, S. J., Yang, D. J., Kang, Materials Chemistry and Physics, **124**, 619 (2010).

[31] A.S., Shaukat, A., Nafady, I., Ullah, Y.H., Taufiq-Yap, I., Shakir, F., Anwar, U., Rashid. Journal of Nanomaterial, 1-6 (2013).

[32] M.A. Rauf, M.A. Meetani, S., Hisaindee. Desalination, **276**, 13 (2011).

[33] C. Grogger, S.G., Fattakhov, V.V., Jouikov, M.M., Shulaeva, V.S. Reznik. ElectrochimicaActa, **49**, 3185 (2004).

[34] P. Christopher, H. Xin, S. Linic. Nat. Chem. **3**, 467 (2011).